

# Giant Out-of-Plane Magnetic Orbital Torque of Altermagnets from Spin-Group Symmetry Breaking

Xukun Feng,<sup>1</sup> Lay Kee Ang,<sup>2</sup> Shengyuan A. Yang,<sup>3,\*</sup> Cong Xiao,<sup>1,†</sup> and X. C. Xie<sup>1,4</sup>

<sup>1</sup>*Interdisciplinary Center for Theoretical Physics and Information Sciences (ICTPIS), Fudan University, Shanghai 200433, China*

<sup>2</sup>*Science, Mathematics and Technology, Singapore University of Technology and Design, Singapore 487372, Singapore*

<sup>3</sup>*Research Laboratory for Quantum Materials, Department of Applied Physics, The Hong Kong Polytechnic University, Kowloon, Hong Kong, China*

<sup>4</sup>*International Center for Quantum Materials, School of Physics, Peking University, Beijing 100871, China*

To search for nontrivial spintronic characters of altermagnets has been a focus in spintronics, with numerous attentions paid to spin-group symmetry dictated non-relativistic effects, such as the spin-splitting torque (SST). Here, we go beyond this paradigm by unveiling the magnetic orbital torque (MOT) that is enabled only by spin-group symmetry breaking of real altermagnets with spin-orbit coupling. This effect enables generating unconventional out-of-plane orbital current with collinear orbital polarization from all 10 spin Laue groups of centrosymmetric altermagnets, which is critical for field-free manipulation of perpendicular magnetization that is a key for next-generation information technology. We reveal perturbative and non-perturbative effects of spin-group symmetry breaking, and unveil that MOT is a much more generic effect of real altermagnets than SST. Our first-principles calculations predict giant out-of-plane MOTs at room temperature in the absence of and competing with SST in experimentally identified altermagnets CrSb and FeSb<sub>2</sub>, respectively. These findings uncover new fundamental physics in altermagnetic spintronics, and open up broad vistas of altermagnets in magnetic memory.

## Introduction

Altermagnets (ATMs) have emerged as a focal point in the study of spintronics and magnetism [1–9]. The non-relativistic spin splitting of ATMs and the underlying spin-group symmetry characters [10–13] have attracted intensive researches that aim at revealing nontrivial spintronic effects [14–20]. A prominent example is the spin-splitting torque (SST), in which a spin Hall current is induced electrically in the absence of spin-orbit coupling (SOC) and then injected into an attached target material to exert a torque [14]. Although attracting immediate experimental interests [21–23], SST is severely limited by spin-group symmetry and can only appear in some classes of *d*-wave ATMs. Therefore, to search for generic spintronic utilities of ATMs in electric control of magnetization remains an open question, which is critical for further development of the field of altermagnetism and its prospects towards applications. In particular, the role of spin-group symmetry breaking due to SOC, which is ubiquitous in real ATMs, in inducing new and qualitatively distinctive torque functionalities has not been explored.

Meanwhile, orbital torque, in which an orbital Hall current is generated electrically and exerts a torque in an attached target, has become another recent focus of spintronics due to the added orbital channel in electric manipulation of magnetization and its great potential for high-efficiency memory devices [24–26]. Up to now, what has been studied in experiments is the orbital torque from nonmagnetic materials made up of light elements [24–35], in which SOC does not have any essential role in generating orbital current [36–39]. Despite intensive researches,

the unconventional out-of-plane orbital torque has not been achieved, which is, however, critical for field-free manipulation and switching of target magnets with perpendicular magnetic anisotropy, a key for scalable high-density magnetic memory and logic devices [40–43].

In this work, we unveil a hidden connection that the desired out-of-plane orbital torque is enabled by the spin-group symmetry breaking in real ATMs with SOC. The key physical mechanism is the magnetic orbital Hall effect, which is odd under time-reversal ( $\mathcal{T}$ ) and need be triggered by SOC, in sharp contrast to the widely studied  $\mathcal{T}$ -even orbital Hall effect in nonmagnetic materials that does not need SOC. The resulting torque is thus termed as magnetic orbital torque (MOT) to be distinguished from the previously studied orbital torque from nonmagnetic materials. The MOT is not shared by collinear antiferromagnets, in which the  $\mathcal{PT}$  ( $\mathcal{P}$  is the inversion) or  $t_{1/2}\mathcal{T}$  ( $t_{1/2}$  is the half-lattice translation) symmetry forbids the magnetic orbital Hall effect in linear response. It is thus a property distinguishing collinear ATMs from antiferromagnets. Importantly, we show that the out-of-plane MOT triggered by spin-group symmetry breaking is allowed in all the ten spin Laue groups of centrosymmetric collinear ATMs, while the out-of-plane SST and orbital torque are only allowed in three and four of the ten, respectively. This universality prompts ATMs as an exceptionally suitable platform for manipulating perpendicular magnetization.

We establish the symmetry structure of MOT from both spin-group and magnetic-group theories, and reveal both perturbative and non-perturbative effects of SOC. We demonstrate our theory in experimentally identified

alters magnetic materials CrSb and FeSb<sub>2</sub>, finding that the MOT in CrSb is mainly contributed by spin-conserving SOC and that in FeSb<sub>2</sub> is mainly from non-perturbative effect of spin-flip SOC. Our first-principles calculations predict giant out-of-plane MOTs at room temperature in both CrSb and FeSb<sub>2</sub>, which surpass the previously reported strongest room-temperature out-of-plane SST [21, 22] and spin-orbit torque (SOT) [44–48]. These findings not only uncover a generic spintronic effect of ATMs with outstanding performance in electric control of magnetization, but also offer new insights into a promising avenue for next-generation ATM-based magnetic memory technology.

## Results and Discussions

### Orbital transport induced by spin-group symmetry breaking

The spin and orbital transport can be expressed as  $j_b^{\chi a} = \sigma_{bc}^{\chi a} E_c$ , where  $\sigma_{bc}^{\chi a}$  is a rank-3 pseudotensor. Here,  $a$  represents the direction of orbital or spin polarization, whereas  $b$  and  $c$  represent the directions of response current and driving field, respectively.  $\chi$  denotes either spin ( $S$ ) or orbital angular momentum ( $L$ ). The spin group symmetries (Methods) determine the response structure of the zeroth-order term  $\sigma_{bc}^{\chi a, (0)}$  in SOC. For spin response, the non-relativistic  $\sigma^{S, (0)}$  may be allowed, underlying the SST [14]. In contrast, the non-relativistic orbital response is forbidden by all collinear ATMs. This is because  $C'_2$  in the spin-only group effectively plays the role of  $\mathcal{T}$  for orbital response, thus prohibits the  $\mathcal{T}$ -odd  $\sigma^{L, (0)}$ . Formally, the action of  $C'_2$  on  $\sigma^{L, (0)}$  yields

$$\sigma_{bc}^{L a, (0)} \xrightarrow{C'_2} -\sigma_{bc}^{L a, (0)}, \quad (1)$$

ensuring that spin-only group symmetry completely prohibits the orbital response. Therefore, the appearance of magnetic orbital Hall effect must require spin-group symmetry breaking by finite SOC.

The spin group symmetry also dictates how  $\sigma^L$  and  $\sigma^S$  are induced by the spin-only group symmetry breaking, provided that SOC is weak compared to other energy scales. In this case, the tensor  $\sigma_{ab}^{\chi c}$  can be expanded in ascending powers of SOC strength. Such an expansion can be made convenient by introducing spin-orbit vector  $\ell^i$  [49] (see Methods), which is defined via  $\sigma = \sigma_i \ell^i$ , where  $\sigma$  is the spin operator and  $i = 1, 2, 3$  labels spin-space directions. Since the order of  $\ell^i$  corresponds to the perturbative order in SOC strength, the expansion can be expressed with respect to  $\ell^i$ :

$$\sigma_{bc}^{\chi a} = \sigma_{bc}^{\chi a, (0)} + \sum_{i;d} \alpha_{bc,d}^{\chi a, i} \ell_d^i + \sum_{ij;de} \beta_{bc,de}^{\chi a, ij} \ell_d^i \ell_e^j + \dots \quad (2)$$

Under a spin-group operation  $[u||R]$ , the spin-orbit vectors transform as  $\ell_a^i \rightarrow \sum_{j;b} \eta_T \det(R) u_{ij} R_{ab} \ell_b^j$ . Combining this transformation rule with Eq. (2) allows one to

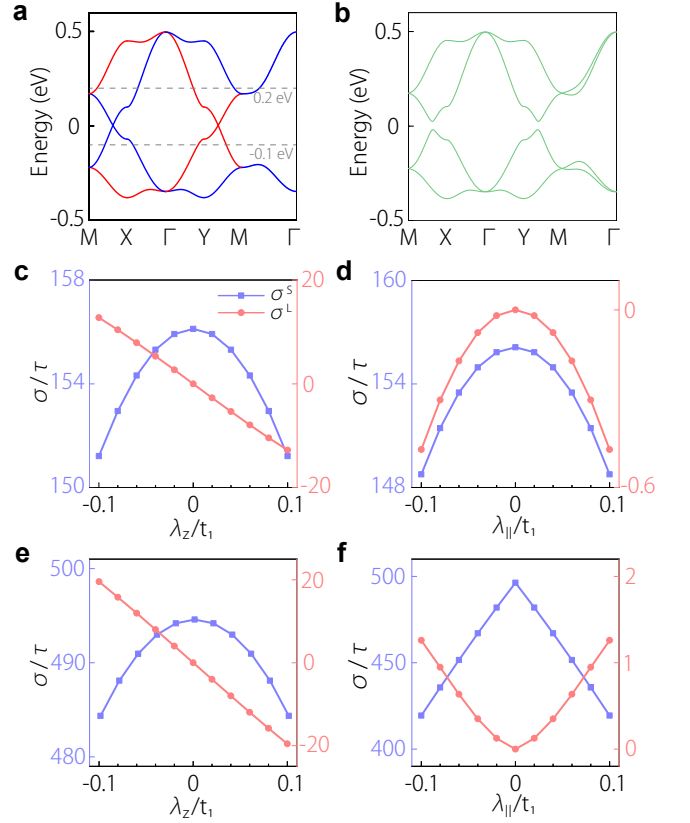


FIG. 1. SOC dependence of magnetic orbital and spin transport in a 2D ATM model (16). **a** Nonrelativistic band structure. Spin-up and -down bands are denoted by red and blue color. **b** Band structure with SOC strength  $\lambda_{||} = \lambda_z = 0.1t_1$ .  $t_1$  is the nearest inter-sublattice hopping. **c** Dependence of  $\sigma^L$  and  $\sigma^S$  on the strength  $\lambda_z$  of spin-conserving SOC, when the spin-flip SOC  $\lambda_{||}$  is turned off.  $\tau$  is the relaxation time. **d** Same as **c**, but with the roles of spin-flip and spin-conserving SOC interchanged. In **c** and **d**, the chemical potential is  $\mu = -0.1$  eV. **e** Same as **c**, with  $\mu = 0.2$  eV. **f** Same as **d**, with  $\mu = 0.2$  eV. The unit of  $\sigma/\tau$  is  $\hbar e^{-1} \Omega^{-1} \text{cm}^{-1} \text{fs}^{-1}$ .

determine the symmetry structures of the magnetic orbital and spin conductivities at any given order of SOC (Eq. (8) in Methods).

For the magnetic orbital conductivity, its expansion in ascending powers of SOC up to the second order is obtained as

$$\sigma_{bc}^{L a} = \alpha_{bc,d}^{L a, 3} \ell_d^3 + \beta_{bc,de}^{L a, 12} (\ell_d^1 \ell_e^2 - \ell_d^2 \ell_e^1). \quad (3)$$

To understand this result, we note that when analyzing the effect of SOC, it is helpful to discern spin-conserving and spin-flip parts of SOC [49–52]. By the construction of spin-orbit vectors,  $\ell^3$  is aligned along the Néel vector in collinear ATMs hence corresponds to spin-conserving SOC, whereas  $\ell^1$  and  $\ell^2$  are for the spin-flip part. Therefore, the first order term of  $\sigma^L$  is related merely to the spin-conserving SOC, whereas the second order term originates solely from the spin-flip SOC.

TABLE I. Symmetry allowed collinearly polarized components of magnetic orbital and spin Hall conductivities [Eq. (2)] for the 10 spin Laue groups relevant to centrosymmetric ATMs. ‘×’ represents the component is forbidden. Here, the spin quantization axis is set to be along the  $z$  direction. The symbols with blue and red colors correspond respectively to collinearly polarized currents parallel and perpendicular to the Néel vector.

Spin Laue Group	Anisotropy	Non-relativistic limit	Spin-conserving SOC	Spin-flip SOC
${}^2m^2m^1m$	$d$ -wave	×	×	×
${}^24/1m$	$d$ -wave	×	$\alpha_{xz,z}^{Lx,3}, \alpha_{yz,z}^{Ly,3}$	$\beta_{xz,xy}^{Lx,12}, \beta_{yz,xy}^{Ly,12}, \alpha_{xz,y}^{Sx,2}, \alpha_{yz,x}^{Sy,1}$
${}^24/1m^2m^1m$	$d$ -wave	×	$\alpha_{xz,z}^{Lx,3}, \alpha_{yz,z}^{Ly,3}$	$\alpha_{xz,y}^{Sx,2}, \alpha_{yz,x}^{Sy,1}, \beta_{xz,xy}^{Lx,12}, \beta_{yz,xy}^{Ly,12}$
${}^14/1m^2m^2m$	$g$ -wave	×	×	×
${}^16/1m^2m^2m$	$i$ -wave	×	×	×
${}^22/2m$	$d$ -wave	$\sigma_{zy}^{S_z,(0)}$	$\alpha_{zy,z}^{Lz,3}, \beta_{zy,zz}^{S_z,33}, \alpha_{xy,z}^{Lx,3}$	$\beta_{zy,xy}^{Lz,12}, \beta_{zy,xx}^{S_z,11}, \beta_{zy,yy}^{S_z,22}, \beta_{xy,xy}^{Lx,12}, \alpha_{xy,y}^{S_x,2}$
${}^1\bar{3}^2m$	$g$ -wave	×	$\alpha_{yx,z}^{Ly,3}$	$\beta_{yx,xy}^{Ly,12}, \alpha_{yx,x}^{Sy,1}$
${}^26/2m$	$g$ -wave	×	$\alpha_{xy,z}^{Lx,3}, \alpha_{yx,z}^{Ly,3}$	$\beta_{xy,xy}^{Lx,12}, \beta_{yx,xy}^{Ly,12}, \alpha_{xy,y}^{S_x,2}, \alpha_{yx,x}^{S_y,1}$
${}^26/2m^2m^1m$	$g$ -wave	×	$\alpha_{xy,z}^{Lx,3}$	$\beta_{xy,xy}^{Lx,12}, \alpha_{xy,y}^{S_x,2}$
${}^1m^1\bar{3}^2m$	$i$ -wave	×	$\alpha_{xz,z}^{Lx,3}, \alpha_{yz,z}^{Ly,3}$	$\alpha_{xz,y}^{S_x,2}, \alpha_{yz,x}^{S_y,1}, \beta_{xz,xy}^{Lx,12}, \beta_{yz,xy}^{Ly,12}$

For the magnetic spin conductivity, the tensor components with spin polarization parallel ( $\parallel$ ) and vertical ( $\perp$ ) to the Néel vector are naturally distinguished in the present framework:

$$\begin{aligned}\sigma_{bc}^{S_{\parallel}} &= \sigma_{bc}^{S_{\parallel},(0)} + \beta_{bc,dd}^{S_{\parallel},33} \ell_d^3 \ell_d^3 + \beta_{bc,ee}^{S_{\parallel},11} \ell_e^1 \ell_e^1 + \beta_{bc,ff}^{S_{\parallel},22} \ell_f^2 \ell_f^2, \\ \sigma_{bc}^{S_{\perp}} &= \alpha_{bc,d}^{S_{\perp},1} \ell_d^1 + \alpha_{bc,f}^{S_{\perp},2} \ell_f^2.\end{aligned}\quad (4)$$

One observes that  $\sigma_{bc}^{S_{\parallel}}$  may be permitted at zeroth order of SOC, which leads to SST, while  $\sigma_{bc}^{S_{\perp},(0)}$  is forbidden by  $C_{\varphi}$  in spin space. Moreover,  $\sigma_{bc}^{S_{\parallel}}$  has no first-order SOC term, but acquires corrections in the second order of both spin-conserving and spin-flip SOC. Meanwhile, since spin-conserving SOC cannot induce  $\sigma_{bc}^{S_{\perp}}$ ,  $\sigma_{bc}^{S_{\perp}}$  is exclusively the result of spin-flip SOC. Spin-group analysis also shows that the second order contribution to  $\sigma_{bc}^{S_{\perp}}$  is prohibited, which is in sharp contrast to  $\sigma^L$  and  $\sigma^{S_{\parallel}}$ .

To illustrate the above generic analysis, we perform numerical calculations in a 2D minimal lattice model with  $d$ -wave altermagnetism as well as spin-conserving and spin-flip SOC [53, 54] (Methods). This model possesses the  $P4mm$  space group, where the Wyckoff position  $2c$  is occupied by  $d_{x^2-y^2}$  orbitals. The nontrivial spin Laue group is  ${}^24/1m^2m^1m$ , and the Néel vector  $\mathbf{N}$  is oriented along  $z$  axis. Figure 1a displays the non-relativistic band structure of the model, with  $d$ -wave altermagnetic spin splitting centered at  $\Gamma$  point, and the band dispersion in the presence of SOC is shown in Fig. 1b. We inspect the components  $\sigma_{xx}^{Lz}$  and  $\sigma_{xx}^{S_z}$  at  $\mu = -0.1$  eV, and separately evaluate the effect of spin-conserving and spin-flip SOC by selectively turning off the other in the Hamiltonian [49–52]. The orbital and spin conductivities are calculated by linear response formulae (Methods). As anticipated,  $\sigma^L$  vanishes in the absence of SOC, and acquires a first-order contribution from spin-conserving SOC ( $\ell_z^3$ ), exhibiting a linear dependence on the corresponding SOC

strength (Fig. 1c). Meanwhile,  $\sigma_{xx}^{S_z}$  survives at the non-relativistic limit and decreases quadratically with the strength of spin-conserving SOC ( $\ell_z^3 \ell_z^3$ ). Spin-flip SOC introduces additional second-order corrections to both  $\sigma_{xx}^{S_z}$  ( $\ell_x^1 \ell_x^1 + \ell_y^2 \ell_y^2$ ) and  $\sigma_{xx}^{Lz}$  ( $\ell_x^1 \ell_y^2$ ), as displayed in Fig. 1d. These results demonstrate that, at  $\mu = -0.1$  eV, the dependence of  $\sigma^{Xz}$  on the SOC strengths follows exactly the perturbative scenario derived from the spin-group analysis.

### Symmetry structures of out-of-plane MOT from ATMs

The above symmetry framework can be used to determine the response structure of magnetic orbital and spin Hall effects with collinearly polarized currents in the 10 spin Laue groups relevant to centrosymmetric ATMs. The results for the case of  $\mathbf{N} \parallel \hat{z}$  are shown in Table I. Noticeably, one sees that the non-relativistic SST component is only allowed in 1 of these 10 classes, with  $d$ -wave anisotropy and low crystallographic symmetry (point group  $2/m$  and halving subgroup  $\bar{1}$ ). In contrast to the stringent limitations on SST, the SOC induced collinearly polarized orbital and spin currents (CPOC and CPSC), with  $a = b$  in  $\sigma_{bc}^{L_a}$  and  $\sigma_{bc}^{S_a}$ , are allowed in 7 of the 10 spin Laue groups. In particular, these conclusions imply that in experimentally identified  $g$ -wave ATM CrSb [55–58] (spin Laue group  ${}^26/2m^2m^1m$ ), and  $d$ -wave ATMs  $\text{KV}_2\text{Se}_2\text{O}$  [59] and  $\text{RbV}_2\text{Te}_2\text{O}$  [60] (spin Laue group  ${}^24/1m^2m^1m$ ), the spin-group symmetry breaking is critical for generating unconventional CPOC and CPSC that are transverse to the Néel vector. Such CPOC and CPSC can induce out-of-plane MOT and SOT on the magnet attached to the ATM.

After considering different orientations of Néel vector ( $\mathbf{N} \parallel \hat{x}$  and  $\mathbf{N} \parallel \hat{y}$ ), we find that the SST is limited to spin Laue groups  ${}^22/2m$ ,  ${}^2m^2m^1m$ , and  ${}^24/1m$  (Supplemen-

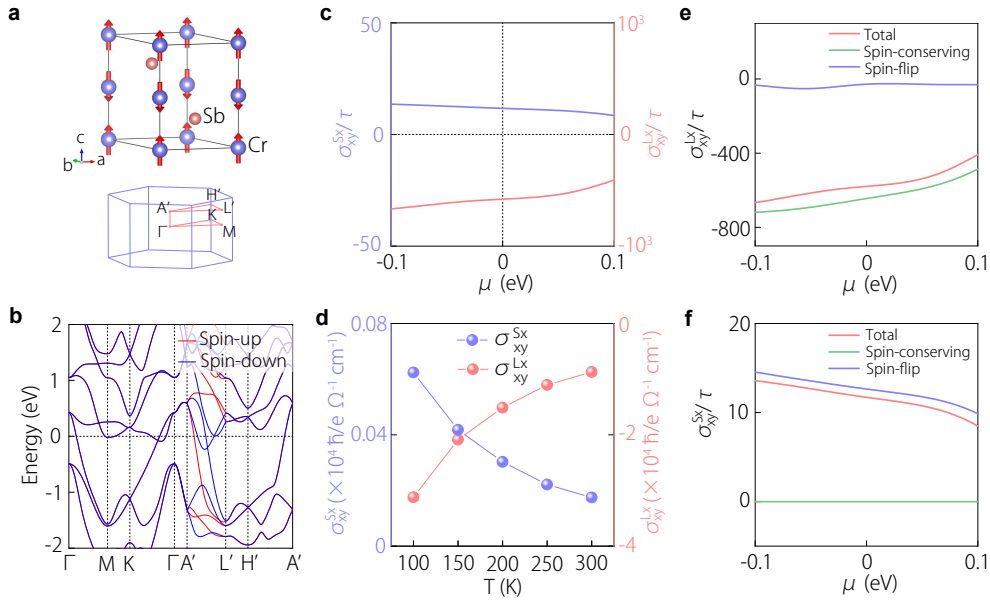


FIG. 2. CPOC and CPSC induced by SOC in CrSb. **a-b** The crystal structure and Brillouin zone (**a**) as well as nonrelativistic band structure (**b**) of CrSb. **c** Calculated  $\sigma_{xy}^{Lx}/\tau$  and  $\sigma_{xy}^{Sx}/\tau$  versus chemical potential. **d**  $\sigma_{xy}^{Lx}$  and  $\sigma_{xy}^{Sx}$  at different temperatures. **e-f** Spin-conserving and spin-flip contributions to magnetic orbital (**e**) and spin (**f**) Hall conductivities.

tary Note 1), while the SOC induced CPOC and CPSC are supported by all the spin Laue groups since the first order of SOC. For example, in the widely studied  $g$ -wave ATM MnTe [61–64] (spin Laue group  $^26/2m^2m^1m$ ), the relativistic CPOC and CPSC dominate. On the other hand, in FeSb<sub>2</sub> [65–67] and Mn<sub>5</sub>Si<sub>3</sub> [68–70] (spin Laue group  $^2m^2m^1m$ ), the relativistic MOT from CPOC coexists with the non-relativistic SST.

### Non-perturbative effects of SOC

Above we have analyzed the spin-group symmetry breaking effect in a perturbative way. Here, we mention possible manifestations of non-perturbative effects of SOC. First of all, we emphasize that the symmetry enforced tensor structures of magnetic orbital and spin Hall conductivities by the perturbative spin-group analysis (Table I, and Supplementary Table S1 and Table S2) remain intact in the non-perturbative magnetic point group analysis (Supplementary Table S3-S5). This consistency confirms the validity of our theory, and implies that non-perturbative effects will not introduce new insights on symmetry properties. Nevertheless, there may be quantitative features of MOT lying outside the perturbative scenario. Particularly, if the perturbative picture always holds, one would expect: (1)  $\sigma^L$  scales linearly with the strength of spin-conserving SOC and quadratically with the spin-flip SOC. (2) The spin-flip SOC contribution to  $\sigma^L$  is always negligible compared to the spin-conserving term. (3) The relativistic CPOC parallel to non-relativistic CPSC is much less than the latter. When the SOC effect is non-perturbative, at least one of these

three expectations will be broken.

The above studied 2D ATM Model provides a specific case of non-perturbative SOC effect. The degeneracy of up- and down-spin bands along M– $\Gamma$  path is protected by the spin-group symmetry [ $C_2 \parallel \mathcal{M}_{xy}$ ], which is broken by the spin-flip SOC, opening a small local gap as shown in Fig. 1b. When the Fermi level locates within the energy window of this local gap, the spin-flip SOC may not behave as a perturbation, although the strength of SOC ( $\lambda$ 's) is much smaller than hopping and exchange energies. Indeed, we perform calculations at such a Fermi level  $\mu = 0.2$  eV, and find that while the spin-conserving SOC contributions to  $\sigma^S$  and  $\sigma^L$  still follow the expectation of perturbation (Fig. 1e), the spin-flip SOC terms of both  $\sigma^S$  or  $\sigma^L$  deviate (Fig. 1f). As we will show, the described non-perturbative scenario may occur in real altermagnetic materials with rich degeneracies in band structures.

### MOT in the absence of SST: CrSb

We now investigate the realization of the above symmetry dictated CPOC in real altermagnetic materials. We first consider the experimentally verified altermagnetic metal CrSb with a Néel temperature of  $\sim 700$  K [55–58]. CrSb crystallizes in the hexagonal space group  $P6_3/mmc$ , with its Néel vector along  $z$  (Fig. 2a) and the spin Laue group  $^26/2m^2m^1m$ . Its non-relativistic band structure (Fig. 2b) displays spin splitting not located at high-symmetry lines in  $k$  space. As mentioned, in the absence of SOC, both CPSC and CPOC are forbidden by spin-group symmetries in CrSb. When SOC is included, the collinearly

TABLE II. Calculated magnetic spin and orbital Hall conductivities (MSHC and MOHC) responsible for CPSC and CPOC, respectively, in CrSb and FeSb<sub>2</sub> at  $T = 300$  K, and corresponding Hall angles. Conductivities are in units of  $(\hbar/e)\Omega^{-1}\text{cm}^{-1}$ .

	CrSb ( $\sigma_{xy}^{x_x}$ )	FeSb <sub>2</sub> ( $\sigma_{yx}^{x_y}$ )	FeSb <sub>2</sub> ( $\sigma_{zx}^{x_z}$ )
MSHC	176	-552	-10
MOHC	-8703	-613	429
SHA	2.0%	-36.3%	-0.7%
OHA	-97.4%	-39.6%	27.6%
EOHA ( $\eta = 38\%$ )	-37.0%	-15.0%	10.5%

polarized component  $\sigma_{xy}^{x_x}$  is allowed according to Table I, which is evaluated by first-principles calculations (calculation details presented in Supplementary Note 5). Figure 2c shows  $\sigma_{xy}^{x_x}/\tau$  as a function of chemical potential at  $T = 300$  K. In a wide energy window around the Fermi level,  $\sigma_{xy}^{L_x}$  and  $\sigma_{xy}^{S_x}$  exhibit opposite signs, and  $\sigma_{xy}^{L_x}$  is about 50 times in magnitude greater than its spin companion. Further, we explore the spin-conserving (spin-flip) contribution by turning off the spin-flip (spin-conserving) SOC, as shown in Fig. 2e and 2f. It is found that the orbital conductivity  $\sigma_{xy}^{L_x}$  is dominated by spin-conserving SOC, whereas the spin conductivity  $\sigma_{xy}^{S_x}$  must require spin-flip SOC, both of which are consistent with our spin-group analysis.

By estimating the relaxation time from experimentally reported longitudinal resistivity  $\rho$  (Supplementary Note 6), we find that at  $T = 300$  K the values of  $\sigma_{xy}^{S_x}$  and  $\sigma_{xy}^{L_x}$  reach 176 and  $-8703$   $(\hbar/e)\Omega^{-1}\text{cm}^{-1}$ , respectively, as shown in Fig. 2d. In comparison, the experimentally reported effective spin Hall conductivities for CPSC thus far are usually less than  $50$   $(\hbar/e)\Omega^{-1}\text{cm}^{-1}$  [47]. A large CPSC about  $100 \sim 200$   $(\hbar/e)\Omega^{-1}\text{cm}^{-1}$  was found recently in nonmagnetic semimetal TaIrTe<sub>4</sub> at room temperature, but is an interface effect [44–46]. To assess the efficiency of spin-to-charge and orbital-to-charge conversion in CrSb, we calculate the spin Hall angle (SHA) and orbital Hall angle (OHA), defined as  $\theta^S = (2e/\hbar)\sigma^S\rho$  and  $\theta^L = (2e/\hbar)\sigma^L\rho$ . The results are summarized in Table II. Notably, the effective orbital Hall angle (EOHA), defined as  $\eta\theta^L$  with  $\eta$  being the orbital-to-spin conversion efficiency of the target materials, can surpass the SHA. For example, it reaches  $-37\%$  when Fe<sub>3</sub>GaTe<sub>2</sub> [35] is considered as the target material ( $\eta = 38\%$ ), which has opposite sign to the SOT and exceeds the latter by more than one order of magnitude. This value is larger than the ever reported strongest out-of-plane SHA (around 10%) [44–48]. Such a large effect reveals that the out-of-plane MOT is exceptionally substantial in manipulating perpendicular magnetization of the target material.

### MOT competing with SST: FeSb<sub>2</sub>

Our second example is FeSb<sub>2</sub>, which crystallizes in the orthorhombic structure with space group  $Pnmm$  and an easy magnetization axis along  $y$ , as illustrated in Fig. 3a. FeSb<sub>2</sub> has been experimentally identified as an ATM with a Néel temperature  $\sim 700$  K [65–67]. The non-relativistic band structure (Fig. 3b) exhibits spin splitting along the  $\Gamma$ -S and R-Z paths. The spin Laue group of FeSb<sub>2</sub> is  $2m^2m^1m$ , which allows the non-relativistic spin conductivity  $\sigma_{yx}^{S_y}$ . In contrast, SOC is essential for a finite orbital term  $\sigma_{yx}^{L_y}$ .

Figure 3c shows the calculated  $\sigma_{yx}^{S_y}$  and  $\sigma_{yx}^{L_y}$  in the presence and absence of SOC at  $T = 300$  K. In the non-relativistic limit,  $\sigma_{yx}^{S_y,(0)}$  is finite, whereas  $\sigma_{yx}^{L_y,(0)}$  is null, in agreement with the spin-group symmetry. Upon introducing SOC,  $\sigma_{yx}^{S_y}$  is not altered much, while  $\sigma_{yx}^{L_y}/\tau$  is significantly increased. By estimating  $\tau$  from the experimental value of resistivity (Supplementary Note 6), we obtain  $\sigma_{yx}^{S_y}$  and  $\sigma_{yx}^{L_y}$  at different temperatures (Fig. 3d), and find that  $\sigma_{yx}^{L_y}$  is a little larger. Particularly, at 300 K,  $\sigma_{yx}^{S_y} = -552$  and  $\sigma_{yx}^{L_y} = -613$   $(\hbar/e)\Omega^{-1}\text{cm}^{-1}$ . The remarkable finding that the relativistic CPOC in FeSb<sub>2</sub> exceeds the non-relativistic CPSC indicates that around the Fermi surface of FeSb<sub>2</sub> SOC may not serve as a perturbation in calculating orbital transport. To explore the origin of this behavior, we calculate the spin-conserving and spin-flip contributions to  $\sigma_{yx}^{L_y}$  in Fig. 3e, finding that the spin-flip term dominates overwhelmingly. This conclusion is consolidated by the  $k$ -resolved integrand maps on the  $k_y = 0$  plane (Figs. 3f and 3g), which also provide further insight: At the non-relativistic limit, the spin-group symmetry  $[C_2||\mathcal{M}_y]$  enforces spin degeneracy on  $k_y = 0$  plane since  $[C_2||\mathcal{M}_y]E(k_x, k_z, s) = E(k_x, k_z, -s)$ , implying a dispersive nodal surface and a nodal line on the Fermi surface. The spin-flip SOC lifts this degeneracy, opening small inter-spin band gaps around the Fermi surface, which strongly enhance second order spin-flip processes. This mechanism is akin to the non-perturbative enhancement proposed in the study of anomalous Hall effect [50, 71, 72], which leads to largely enhanced Hall conductivity from spin-flip processes when the Fermi level locates within the local inter-spin gaps [50, 72].

Because of the ubiquitous presence of spin-group protected degeneracy that can be broken by spin-flip SOC in ATMs, such non-perturbative SOC effects may be generally expected, provided that this type of degeneracy appears around the Fermi surface.

Additionally, the symmetry analysis predicts that in FeSb<sub>2</sub> SOC activates  $\sigma_{zx}^{S_z}$  and  $\sigma_{zx}^{L_z}$ .  $\sigma_{zx}^{S_z}$  can only arise from spin-flip SOC, whereas  $\sigma_{zx}^{L_z}$  can be from both spin-conserving and spin-flip SOC. The calculated results for them are presented in Fig. 3d. At 300 K,  $\sigma_{zx}^{S_z}$  and  $\sigma_{zx}^{L_z}$  reach  $-10$  and  $429$   $(\hbar/e)\Omega^{-1}\text{cm}^{-1}$ , respectively, showing again that the SOC induced CPOC perpendicular to the Néel vector can significantly exceed its spin counterpart.

Lastly, we evaluate the SHA and EOHA of FeSb<sub>2</sub>, as

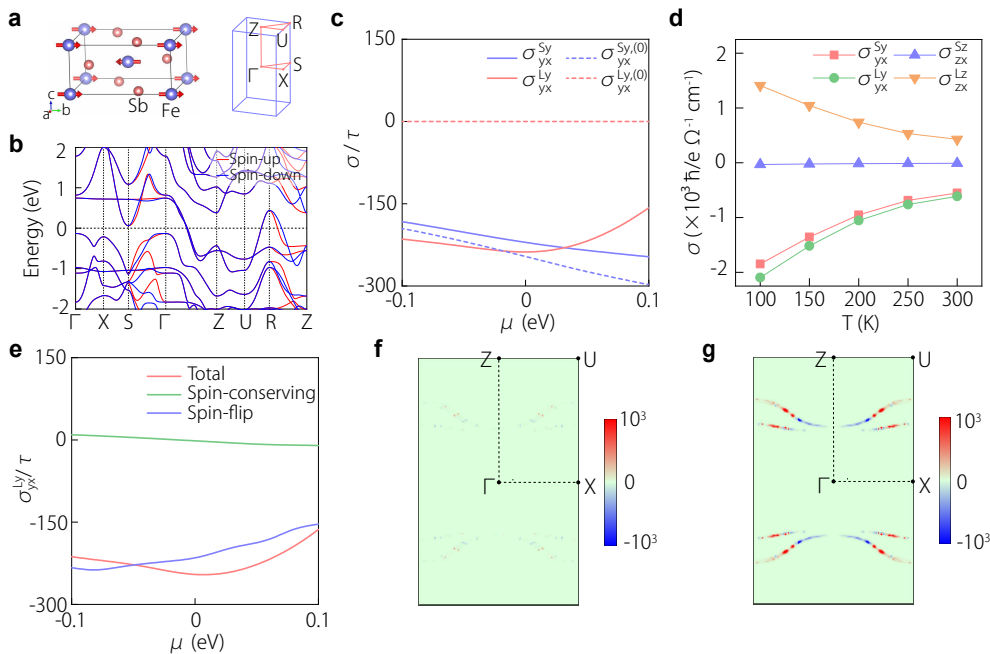


FIG. 3. SOC induced CPOC competing with non-relativistic CPSC in FeSb<sub>2</sub>. **a** Crystal structure and Brillouin zone of FeSb<sub>2</sub>. **b** The non-relativistic band structure of FeSb<sub>2</sub>. **c** Calculated  $\sigma_{yx}^{L_y}/\tau$  and  $\sigma_{yx}^{S_y}/\tau$  versus chemical potential. **d** Magnetic orbital and spin Hall conductivities at different temperatures, with orbital and spin polarizations both parallel and transverse to  $\mathbf{N}$ . **e** Spin-conserving and spin-flip contributions to  $\sigma_{yx}^{L_y}$ . **f-g** Spin-conserving (**f**) and spin-flip (**g**) contributions to  $k$ -resolved  $\sigma_{yx}^{L_y}$  on the  $k_y = 0$  plane.

summarized in Table II. The SHA  $\theta_{yx}^{S_y}$ , which leads to SST with small SOT correction (Fig. 3c), is  $-36.3\%$ , whereas the OHA  $\theta_{yx}^{L_y} = -39.6\%$  is a little larger. If the spin target material has sizable orbital-to-spin conversion efficiency  $\eta$ , the MOT from such an OHA can have a comparable efficiency to the SST. For the case of Fe<sub>3</sub>GaTe<sub>2</sub> [35] as the target, the EOHA  $\eta\theta_{yx}^{L_y}$  of FeSb<sub>2</sub> attains  $-15.0\%$ , which is indeed comparable to the SST. In target materials with larger  $\eta$  [33], the value of induced MOT from FeSb<sub>2</sub> can be closer to the SST.

In summary, we have revealed that SOC presented in real altermagnetic materials unlocks the unconventional out-of-plane MOT, which heralds unprecedented possibilities of ATMs as high-efficiency platforms for scalable high-density spintronic memory devices integrating perpendicular magnetic anisotropy. In particular, the significant room-temperature out-of-plane MOT predicted by first-principles calculations in CrSb has the opposite sign to the much smaller out-of-plane SOT, without the accompany of SST and orbital torque (see Supplementary Note 3 for the symmetry analysis on CPOC from  $\mathcal{T}$ -even orbital Hall effect in ATMs), rendering an excellent platform for experimental detection. These findings unveil the active and significant role of spin-group symmetry breaking in altermagnetic spintronics, and will stimulate broad explorations into the impact of this symmetry breaking on linear and nonlinear electric manipulation of magnetism via coupled spin and orbital degrees

of freedom.

## Methods

### Notations of Spin group

A spin group is the direct product of a nonrelativistic spin-only group  $\mathbf{r}_s$  and a nontrivial spin group  $\mathbf{R}_s$  [1]. It consists of composite operations  $[u||R]$ , where  $u$  and  $R$  act respectively in spin and real space. For collinear altermagnets,  $\mathbf{r}_s$  is generated by  $[C_2||E]$  and  $[C_\varphi||E]$  symmetries. Here,  $[C_2||E]$  denotes a twofold spin-space rotation about an axis perpendicular to the Néel vector, combined with time-reversal  $\mathcal{T}$  as spin-space inversion. Note that  $\mathcal{T}$  can flip the sign of momentum [1].  $[C_\varphi||E]$  represents a spin-space rotation around the Néel vector with an arbitrary angle  $\varphi$ . In altermagnets,  $\mathbf{R}_s$  can be described by the third type of spin Laue group  $\mathbf{R}_s^{\text{III}}$ , which can be expressed as [1]  $\mathbf{R}_s^{\text{III}} = [E||\mathbf{H}] + [C_2||A][E||\mathbf{H}] = [E||\mathbf{H}] + [C_2||(\mathbf{G} - \mathbf{H})]$ , where  $\mathbf{G}$  is the crystallographic Laue group,  $\mathbf{H}$  is the subgroup of  $\mathbf{G}$  includes real-space operations connecting the same spin sublattices, whereas  $[C_2||A]$  links the opposite spin sublattices.

### An explanation on spin-orbit vector

Following Ref. [49], the spin-orbit coupling can be ex-

pressed in a tensorial form as

$$\hat{H}_{\text{SOC}} = \frac{\hbar}{m^2 c^2} \sum_{i=1}^3 (\boldsymbol{\ell}^i \cdot \hat{\mathbf{O}}) \sigma_i, \quad (5)$$

where  $\hat{\mathbf{O}} \propto \nabla V \times \mathbf{p}$  is the orbital operator acting in real space, and  $\boldsymbol{\sigma} = (\sigma_1, \sigma_2, \sigma_3)$  are the Pauli matrices in spin space. The three vectors  $\{\boldsymbol{\ell}^i\}$  are referred to as the *spin-orbit vectors*. Each  $\boldsymbol{\ell}^i$  maps the  $i$ -th orthonormal basis of the spin space (also called the ‘‘color space’’) onto the crystal coordinate frame, thereby manifesting the relative orientation between the spin and lattice coordinate systems. As illustrated in Supplementary Fig. S1, the relative alignment of the spin and crystal frames can be described by three Euler angles ( $\phi$ ,  $\theta$ , and  $\varphi$ ). Hence, the spin-orbit vectors are given by  $\boldsymbol{\ell}^1 = (\cos \phi \cos \varphi - \cos \theta \sin \phi \sin \varphi, \sin \phi \cos \varphi + \cos \theta \cos \phi \sin \varphi, \sin \theta \sin \varphi)$ ,  $\boldsymbol{\ell}^2 = (-\cos \phi \sin \varphi - \cos \theta \sin \phi \cos \varphi, -\sin \phi \sin \varphi + \cos \theta \cos \phi \cos \varphi, \sin \theta \cos \varphi)$  and  $\boldsymbol{\ell}^3 = (\sin \theta \sin \phi, -\sin \theta \cos \phi, \cos \theta)$ . The set  $\{\boldsymbol{\ell}^i\}$  thus connects the spin space to the crystal space, satisfying the orthonormality relations  $\ell_a^i \ell_b^i = \delta_{ab}$  and  $\ell_a^i \ell_a^j = \delta_{ij}$ . Take the collinear altermagnet FeSb<sub>2</sub> as an example, whose Néel vector along the  $y$  axis of the crystal frame, the Néel vector is defined to lie along the  $z$  axis of the spin frame, leading to  $\theta = -\pi/2$  and  $\phi = 0$ . The Euler angle  $\varphi$  can be set to zero without loss of generality owing to its gauge freedom. Under these conditions, the three spin-orbit vectors of FeSb<sub>2</sub> are  $\boldsymbol{\ell}^1 = (1, 0, 0)$ ,  $\boldsymbol{\ell}^2 = (0, 0, -1)$ , and  $\boldsymbol{\ell}^3 = (0, 1, 0)$ .

### Spin-group symmetry transformations of orbital and spin conductivities

Under a spin-group operation  $[u||R]$ , the zeroth-order magnetic spin and orbital conductivities transform as (the Einstein summation convention for Cartesian indices is implied henceforth)

$$\begin{aligned} \sigma_{bc}^{S_{a'},(0)} &= u_{aa'} R_{bb'} R_{cc'} \sigma_{b'c'}^{S_{a'},(0)}, \\ \sigma_{bc}^{L_{a'},(0)} &= \eta_T \det(R) R_{aa'} R_{bb'} R_{cc'} \sigma_{b'c'}^{L_{a'},(0)}, \end{aligned} \quad (6)$$

where  $\eta_T = +1$  ( $-1$ ) for symmetry operations without (with)  $\mathcal{T}$ . The sharply different transformation rules of spin and orbital responses imply distinct symmetry characters of them.

Under a general spin-group operation  $[u||R]$ , the spin-orbit vectors transform as

$$\ell_a^i \longrightarrow \eta_T \det(R) u_{ij} R_{ab} \ell_b^j, \quad (7)$$

where  $\eta = \pm 1$  denotes the presence or absence of time reversal. Consequently,  $\alpha_{bc,d}^{\chi_{a'},i}$  and  $\beta_{bc,de}^{\chi_{a'},ij}$  in Eq. (2) trans-

form as

$$\begin{aligned} \alpha_{bc,d}^{S_{a'},i} &= \eta_T \det(R) u_{aa'} R_{bb'} R_{cc'} R_{dd'} u_{ii'} \alpha_{b'c',d'}^{S_{a'},i'}, \\ \beta_{bc,de}^{S_{a'},ij} &= u_{aa'} R_{bb'} R_{cc'} R_{dd'} R_{ee'} u_{ii'} u_{jj'} \beta_{b'c',d'e'}^{S_{a'},i'j'}, \\ \alpha_{bc,d}^{L_{a'},i} &= R_{aa'} R_{bb'} R_{cc'} R_{dd'} u_{ii'} \alpha_{b'c',d'}^{L_{a'},i'}, \\ \beta_{bc,de}^{L_{a'},ij} &= \eta_T \det(R) R_{aa'} R_{bb'} R_{cc'} R_{dd'} R_{ee'} u_{ii'} u_{jj'} \beta_{b'c',d'e'}^{L_{a'},i'j'}. \end{aligned} \quad (8)$$

We further show that, from the first transformation rule in Eq. (8), the first-order SOC correction  $\alpha_{bc,d}^{S_{a'},i}$  is forbidden for both spin-conserving and spin-flip SOC. The representation matrix of the  $C_\varphi$  symmetry is

$$u(C_\varphi) = \begin{pmatrix} \cos \varphi & -\sin \varphi & 0 \\ \sin \varphi & \cos \varphi & 0 \\ 0 & 0 & 1 \end{pmatrix}. \quad (9)$$

Thus, the  $u_{aa'}$  in Eq. (8) has the form

$$u_{|||} = 1, \quad u_{||a'} = 0 \quad (a' \neq ||), \quad (10)$$

so that  $u_{aa'} = u_{||a'} = \delta_{||,a'}$ . Thus the first transformation equation in Eq. (8) reduces to

$$\alpha_{bc,d}^{S_{||},i} = \eta_T R_{bb'} R_{cc'} R_{dd'} u_{ii'} \alpha_{b'c',d'}^{S_{||},i'}. \quad (11)$$

For the spin-flip SOC, we have  $i \neq ||$  and  $i' \neq ||$ . Because  $\alpha_{bc,d}^{S_{||},i}$  is not invariant under  $C_\varphi$ , all first-order contributions from spin-flip SOC are forbidden,

$$\alpha_{bc,d}^{S_{||},i} = 0, \quad (i \neq ||). \quad (12)$$

For the spin-conserving SOC, the transformation simplifies further to

$$\alpha_{bc,d}^{S_{||},||} = \eta_T R_{bb'} R_{cc'} R_{dd'} \alpha_{b'c',d'}^{S_{||},||}. \quad (13)$$

Here the operation  $C'_2$  acts as an effective time-reversal symmetry on  $\alpha_{bc,d}^{S_{||},||}$ , which forces

$$\alpha_{bc,d}^{S_{||},||} = 0. \quad (14)$$

Therefore, both the spin-flip and spin-conserving SOC are prohibited at first order by the spin group symmetries  $C_\varphi$  and  $C'_2$ , respectively. As a result,  $\sigma^{S_{||}}$  at the non-relativistic limit cannot acquire any correction in the first order of SOC.

Furthermore, we show that, the SOC correction to  $\sigma_{bc}^{S_{||}^{\perp}}$  begins at first order in the spin-flip SOC, while the second-order correction from spin-flip SOC is forbidden due to the constraint of the  $C'_2$  symmetry. Without loss of generality, we set the spin quantization axis along the  $x$  or  $y$  direction in spin space, thus the representation matrix of  $C'_2$  is given by

$$u(C'_2) = - \begin{pmatrix} 1 & 0 & 0 \\ 0 & -1 & 0 \\ 0 & 0 & -1 \end{pmatrix} \text{ or } - \begin{pmatrix} -1 & 0 & 0 \\ 0 & 1 & 0 \\ 0 & 0 & -1 \end{pmatrix} \quad (15)$$

In this symmetry setting, second-order spin-flip correction to  $\sigma^{S\perp}$  is prohibited, while the first-order correction from spin-flip SOC is allowed.

## 2D ATM model

To verify the above analysis, we perform numerical calculations in a 2D minimal lattice model exhibiting  $d$ -wave altermagnetism [53, 54]. This model possesses the  $P4mm$  space group, where the Wyckoff position  $2c$  is occupied by  $d_{x^2-y^2}$  orbitals. The nontrivial spin Laue group is  $^2_4/1m^2m^1m$ . The Hamiltonian reads

$$\mathcal{H} = \mathcal{H}_0 + \mathcal{H}_{\text{SOC}}. \quad (16)$$

Here, the nonrelativistic Hamiltonian  $\mathcal{H}_0$  is given by

$$\begin{aligned} \mathcal{H}_0 = & 4t_1 c_{x/2} c_{y/2} \tau_x + 2t_2 (c_x + c_y) \tau_0 \\ & + 2t_d (c_x - c_y) \tau_z + J \tau_z \mathbf{N} \cdot \sigma, \end{aligned} \quad (17)$$

where  $c_{a/n} \equiv \cos(k_a/n)$  and  $s_{a/n} \equiv \sin(k_a/n)$ ,  $\tau$  and  $\sigma$  the sublattice and spin Pauli matrices, respectively.  $t_1$  represents the nearest inter-sublattice hopping, whereas  $t_2$  and  $t_d$  are intra-sublattice hopping parameters, with  $t_d$  controlling the nonrelativistic spin splitting. We set the Néel vector along  $z$  direction with SOC, thus the antiferromagnetic coupling term is  $J \tau_z \sigma_z$ . The SOC Hamiltonian includes spin-conserving and spin-flip parts:

$$\begin{aligned} \mathcal{H}_C &= 4\lambda_z s_{x/2} s_{y/2} \tau_y \sigma_z, \\ \mathcal{H}_F &= 4\lambda_{\parallel} (s_{x/2} c_{y/2} \tau_y \sigma_x + c_{x/2} s_{y/2} \tau_y \sigma_y). \end{aligned} \quad (18)$$

In the calculation shown in Fig. 1, we take  $4t_1 = 0.4$ ,  $2t_2 = -0.025$ ,  $2t_d = -0.125$ , and  $J = 0.165$ . With the Néel vector oriented along  $z$ , the spin-orbit vectors are  $\ell^1 = (1, 0, 0)$ ,  $\ell^2 = (0, 1, 0)$ , and  $\ell^3 = (0, 0, 1)$ , corresponding respectively to spin-flip ( $\ell^{1,2}$ ) and spin-conserving ( $\ell^3$ ) SOC.

## Transport formulation

The spin and orbital currents can be expressed as

$$\mathbf{j}^{\chi c} = \frac{e}{\hbar} \sum_n \int \frac{d^3 \mathbf{k}}{(2\pi)^3} f_n(\mathbf{k}) \mathbf{j}_n^{\chi c}(\mathbf{k}), \quad (19)$$

where  $n$  and  $\mathbf{k}$  are the band index and crystal momentum, respectively,  $\mathbf{j}_n^{\chi c}(\mathbf{k}) = \langle u_n(\mathbf{k}) | \frac{1}{2} \{ \hat{\mathbf{v}}, \hat{\chi}^c \} | u_n(\mathbf{k}) \rangle$  is the intraband matrix element of the spin or orbital current operator. Here, the matrix element of orbital angular momentum in the band representation is [38, 73–75]

$$\mathbf{L}_{mn} = \frac{ie\hbar^2}{4\mu_B} \sum_{p \neq m, n} \left( \frac{1}{\varepsilon_{pm}} + \frac{1}{\varepsilon_{pn}} \right) \mathbf{v}_{mp} \times \mathbf{v}_{pn}, \quad (20)$$

where  $\mu_B$  is the Bohr magneton. With relaxation time approximation the nonequilibrium Fermi distribution is given by  $f_n - f_0 = \frac{e}{\hbar} \tau \mathbf{E} \cdot \partial_{\mathbf{k}} f_0$ . Hence, the MSHC and MOHC can be expressed as

$$\sigma_{ab}^{\chi c} = \frac{e^2}{\hbar} \tau \sum_n \int \frac{d^3 \mathbf{k}}{(2\pi)^3} (-\partial_{\varepsilon} f_0) j_a^{\chi c}(\mathbf{k}) v_b(\mathbf{k}) \quad (21)$$

where  $v_b$  is group velocity along  $b$  direction.

\* shengyuan.yang@polyu.edu.hk

† congxiao@fudan.edu.cn

- [1] L. Šmejkal, J. Sinova, and T. Jungwirth, Beyond conventional ferromagnetism and antiferromagnetism: A phase with nonrelativistic spin and crystal rotation symmetry, *Phys. Rev. X* **12**, 031042 (2022).
- [2] L. Šmejkal, J. Sinova, and T. Jungwirth, Emerging research landscape of altermagnetism, *Phys. Rev. X* **12**, 040501 (2022).
- [3] C. Wu, K. Sun, E. Fradkin, and S.-C. Zhang, Fermi liquid instabilities in the spin channel, *Phys. Rev. B* **75**, 115103 (2007).
- [4] M. Naka, S. Hayami, H. Kusunose, Y. Yanagi, Y. Motome, and H. Seo, Spin current generation in organic antiferromagnets, *Nat. Commun.* **10**, 4305 (2019).
- [5] S. Hayami, Y. Yanagi, and H. Kusunose, Momentum-dependent spin splitting by collinear antiferromagnetic ordering, *J. Phys. Soc. Jpn.* **88**, 123702 (2019).
- [6] L. Šmejkal, R. González-Hernández, T. Jungwirth, and J. Sinova, Crystal time-reversal symmetry breaking and spontaneous hall effect in collinear antiferromagnets, *Sci. Adv.* **6**, eaaz8809 (2020).
- [7] L.-D. Yuan, Z. Wang, J.-W. Luo, E. I. Rashba, and A. Zunger, Giant momentum-dependent spin splitting in centrosymmetric low- $z$  antiferromagnets, *Phys. Rev. B* **102**, 014422 (2020).
- [8] D.-F. Shao, S.-H. Zhang, M. Li, C.-B. Eom, and E. Y. Tsymlal, Spin-neutral currents for spintronics, *Nat. Commun.* **12**, 7061 (2021).
- [9] H.-Y. Ma, M. Hu, N. Li, J. Liu, W. Yao, J.-F. Jia, and J. Liu, Multifunctional antiferromagnetic materials with giant piezomagnetism and noncollinear spin current, *Nat. Commun.* **12**, 2846 (2021).
- [10] P. Liu, J. Li, J. Han, X. Wan, and Q. Liu, Spin-group symmetry in magnetic materials with negligible spin-orbit coupling, *Phys. Rev. X* **12**, 021016 (2022).
- [11] Z. Xiao, J. Zhao, Y. Li, R. Shindou, and Z.-D. Song, Spin space groups: Full classification and applications, *Phys. Rev. X* **14**, 031037 (2024).
- [12] Y. Jiang, Z. Song, T. Zhu, Z. Fang, H. Weng, Z.-X. Liu, J. Yang, and C. Fang, Enumeration of spin-space groups: Toward a complete description of symmetries of magnetic orders, *Phys. Rev. X* **14**, 031039 (2024).
- [13] H. Zhu, J. Li, X. Chen, Y. Yu, and Q. Liu, Magnetic geometry induced quantum geometry and nonlinear transports, *Nat. Commun.* **16**, 4882 (2025).
- [14] R. González-Hernández, L. Šmejkal, K. Vybourný, Y. Yanagi, J. Sinova, T. c. v. Jungwirth, and J. Železný, Efficient electrical spin splitter based on nonrelativistic collinear antiferromagnetism, *Phys. Rev. Lett.* **126**, 127701 (2021).
- [15] L. Šmejkal, A. B. Hellenes, R. González-Hernández, J. Sinova, and T. Jungwirth, Giant and tunneling magnetoresistance in unconventional collinear antiferromagnets with nonrelativistic spin-momentum coupling, *Phys. Rev. X* **12**, 011028 (2022).
- [16] D.-F. Shao, Y.-Y. Jiang, J. Ding, S.-H. Zhang, Z.-A. Wang, R.-C. Xiao, G. Gurung, W. J. Lu, Y. P. Sun, and

- E. Y. Tsymbal, Néel spin currents in antiferromagnets, *Phys. Rev. Lett.* **130**, 216702 (2023).
- [17] L. Bai, W. Feng, S. Liu, L. Šmejkal, Y. Mokrousov, and Y. Yao, Altermagnetism: Exploring new frontiers in magnetism and spintronics, *Adv. Funct. Mater.* **34**, 2409327 (2024).
- [18] R.-W. Zhang, C. Cui, R. Li, J. Duan, L. Li, Z.-M. Yu, and Y. Yao, Predictable gate-field control of spin in altermagnets with spin-layer coupling, *Phys. Rev. Lett.* **133**, 056401 (2024).
- [19] C. Song, H. Bai, Z. Zhou, L. Han, H. Reichlova, J. H. Dil, J. Liu, X. Chen, and F. Pan, Altermagnets as a new class of functional materials, *Nat. Rev. Mater.* **10**, 473 (2025).
- [20] J. Lai, T. Yu, P. Liu, L. Liu, G. Xing, X.-Q. Chen, and Y. Sun,  $d$ -wave flat fermi surface in altermagnets enables maximum charge-to-spin conversion, *Phys. Rev. Lett.* **135**, 256702 (2025).
- [21] A. Bose, N. J. Schreiber, R. Jain, D.-F. Shao, H. P. Nair, J. Sun, X. S. Zhang, D. A. Muller, E. Y. Tsymbal, D. G. Schlom, *et al.*, Tilted spin current generated by the collinear antiferromagnet ruthenium dioxide, *Nat. Electron.* **5**, 267 (2022).
- [22] S. Karube, T. Tanaka, D. Sugawara, N. Kadoguchi, M. Kohda, and J. Nitta, Observation of spin-splitter torque in collinear antiferromagnetic  $\text{ruo}_2$ , *Phys. Rev. Lett.* **129**, 137201 (2022).
- [23] H. Bai, Y. C. Zhang, Y. J. Zhou, P. Chen, C. H. Wan, L. Han, W. X. Zhu, S. X. Liang, Y. C. Su, X. F. Han, F. Pan, and C. Song, Efficient spin-to-charge conversion via altermagnetic spin splitting effect in antiferromagnet  $\text{ruo}_2$ , *Phys. Rev. Lett.* **130**, 216701 (2023).
- [24] D. Lee, D. Go, H.-J. Park, W. Jeong, H.-W. Ko, D. Yun, D. Jo, S. Lee, G. Go, J. H. Oh, *et al.*, Orbital torque in magnetic bilayers, *Nat. Commun.* **12**, 6710 (2021).
- [25] Y.-G. Choi, D. Jo, K.-H. Ko, D. Go, K.-H. Kim, H. G. Park, C. Kim, B.-C. Min, G.-M. Choi, and H.-W. Lee, Observation of the orbital hall effect in a light metal ti, *Nature* **619**, 52 (2023).
- [26] S. Ding, M.-G. Kang, W. Legrand, and P. Gambardella, Orbital torque in rare-earth transition-metal ferrimagnets, *Phys. Rev. Lett.* **132**, 236702 (2024).
- [27] Z. C. Zheng, Q. X. Guo, D. Jo, D. Go, L. H. Wang, H. C. Chen, W. Yin, X. M. Wang, G. H. Yu, W. He, H.-W. Lee, J. Teng, and T. Zhu, Magnetization switching driven by current-induced torque from weakly spin-orbit coupled zr, *Phys. Rev. Res.* **2**, 013127 (2020).
- [28] D. Go and H.-W. Lee, Orbital torque: Torque generation by orbital current injection, *Phys. Rev. Res.* **2**, 013177 (2020).
- [29] S. Ding, A. Ross, D. Go, L. Baldrati, Z. Ren, F. Freimuth, S. Becker, F. Kammerbauer, J. Yang, G. Jakob, Y. Mokrousov, and M. Kläui, Harnessing orbital-to-spin conversion of interfacial orbital currents for efficient spin-orbit torques, *Phys. Rev. Lett.* **125**, 177201 (2020).
- [30] J. Kim, D. Go, H. Tsai, D. Jo, K. Kondou, H.-W. Lee, and Y. Otani, Nontrivial torque generation by orbital angular momentum injection in ferromagnetic-metal/Cu/al<sub>2</sub>o<sub>3</sub> trilayers, *Phys. Rev. B* **103**, L020407 (2021).
- [31] S. Lee, M.-G. Kang, D. Go, D. Kim, J.-H. Kang, T. Lee, G.-H. Lee, J. Kang, N. J. Lee, Y. Mokrousov, *et al.*, Efficient conversion of orbital hall current to spin current for spin-orbit torque switching, *Commun. Phys.* **4**, 234 (2021).
- [32] Z. Zheng, T. Zeng, T. Zhao, S. Shi, L. Ren, T. Zhang, L. Jia, Y. Gu, R. Xiao, H. Zhou, *et al.*, Effective electrical manipulation of a topological antiferromagnet by orbital torques, *Nat. Commun.* **15**, 745 (2024).
- [33] Y. Yang, P. Wang, J. Chen, D. Zhang, C. Pan, S. Hu, T. Wang, W. Yue, C. Chen, W. Jiang, *et al.*, Orbital torque switching in perpendicularly magnetized materials, *Nat. Commun.* **15**, 8645 (2024).
- [34] R. Gupta, C. Bouard, F. Kammerbauer, J. O. Ledesma-Martin, A. Bose, I. Kononenko, S. Martin, P. Usé, G. Jakob, M. Drouard, *et al.*, Harnessing orbital hall effect in spin-orbit torque mram, *Nat. Commun.* **16**, 130 (2025).
- [35] D. Zhang, H. Wei, J. Duan, J. Chen, J. Chen, D. Yue, W. Gong, P. Liu, Y. Yang, J. Gou, *et al.*, Orbital torque switching of room temperature two-dimensional van der waals ferromagnet fe<sub>3</sub>gate<sub>2</sub>, *Nat. Commun.* **16**, 7047 (2025).
- [36] D. Go, D. Jo, C. Kim, and H.-W. Lee, Intrinsic spin and orbital hall effects from orbital texture, *Phys. Rev. Lett.* **121**, 086602 (2018).
- [37] D. Jo, D. Go, and H.-W. Lee, Gigantic intrinsic orbital hall effects in weakly spin-orbit coupled metals, *Phys. Rev. B* **98**, 214405 (2018).
- [38] A. Pezo, D. García Ovalle, and A. Manchon, Orbital hall effect in crystals: Interatomic versus intra-atomic contributions, *Phys. Rev. B* **106**, 104414 (2022).
- [39] I. Lyalin, S. Alikhah, M. Berritta, P. M. Oppeneer, and R. K. Kawakami, Magneto-optical detection of the orbital hall effect in chromium, *Phys. Rev. Lett.* **131**, 156702 (2023).
- [40] H. Kurebayashi, Going in the right direction, *Nat. Phys.* **13**, 209 (2017).
- [41] A. Manchon, J. Železný, I. M. Miron, T. Jungwirth, J. Sinova, A. Thiaville, K. Garello, and P. Gambardella, Current-induced spin-orbit torques in ferromagnetic and antiferromagnetic systems, *Rev. Mod. Phys.* **91**, 035004 (2019).
- [42] J. Ryu, S. Lee, K.-J. Lee, and B.-G. Park, Current-induced spin-orbit torques for spintronic applications, *Adv. Mater.* **32**, 1907148 (2020).
- [43] H. Yang and Y. Liu, Field-free and unconventional switching of perpendicular magnetization at room temperature, *Nat. Electron.* **6**, 724 (2023).
- [44] Y. Liu, G. Shi, D. Kumar, T. Kim, S. Shi, D. Yang, J. Zhang, C. Zhang, F. Wang, S. Yang, *et al.*, Field-free switching of perpendicular magnetization at room temperature using out-of-plane spins from tairte<sub>4</sub>, *Nat. Electron.* **6**, 732 (2023).
- [45] Y. Zhang, H. Xu, K. Jia, G. Lan, Z. Huang, B. He, C. He, Q. Shao, Y. Wang, M. Zhao, *et al.*, Room temperature field-free switching of perpendicular magnetization through spin-orbit torque originating from low-symmetry type ii weyl semimetal, *Sci. Adv.* **9**, eadg9819 (2023).
- [46] L. Bainsla, B. Zhao, N. Behera, A. M. Hoque, L. Sjöström, A. Martinelli, M. Abdel-Hafiez, J. Åkerman, and S. P. Dash, Large out-of-plane spin-orbit torque in topological weyl semimetal tairte<sub>4</sub>, *Nat. Commun.* **15**, 4649 (2024).
- [47] F. Wang, G. Shi, K.-W. Kim, H.-J. Park, J. G. Jang, H. R. Tan, M. Lin, Y. Liu, T. Kim, D. Yang, *et al.*, Field-free switching of perpendicular magnetization by two-dimensional pttte<sub>2</sub>/wte<sub>2</sub> van der waals heterostruc-

- tures with high spin hall conductivity, *Nat. Mater.* **23**, 768 (2024).
- [48] I. Abdelwahab, D. Kumar, T. Bian, H. Zheng, H. Gao, F. Hu, A. McClelland, K. Leng, W. L. Wilson, J. Yin, *et al.*, Two-dimensional chiral perovskites with large spin hall angle and collinear spin hall conductivity, *Science* **385**, 311 (2024).
- [49] Z. Liu, M. Wei, W. Peng, D. Hou, Y. Gao, and Q. Niu, Multipolar anisotropy in anomalous hall effect from spin-group symmetry breaking, *Phys. Rev. X* **15**, 031006 (2025).
- [50] H. Zhang, F. Freimuth, S. Blugel, Y. Mokrousov, and I. Souza, Role of spin-flip transitions in the anomalous hall effect of fept alloy, *Phys. Rev. Lett.* **106**, 117202 (2011).
- [51] G. Y. Guo, Q. Niu, and N. Nagaosa, Anomalous nernst and hall effects in magnetized platinum and palladium, *Phys. Rev. B* **89**, 214406 (2014).
- [52] M. Roig, Y. Yu, R. C. Ekman, A. Kreisel, B. M. Andersen, and D. F. Agterberg, Quasisymmetry-constrained spin ferromagnetism in altermagnets, *Phys. Rev. Lett.* **135**, 016703 (2025).
- [53] M. Roig, A. Kreisel, Y. Yu, B. M. Andersen, and D. F. Agterberg, Minimal models for altermagnetism, *Phys. Rev. B* **110**, 144412 (2024).
- [54] D. S. Antonenko, R. M. Fernandes, and J. W. Venderbos, Mirror chern bands and weyl nodal loops in altermagnets, *Phys. Rev. Lett.* **134**, 096703 (2025).
- [55] S. Reimers, L. Odenbreit, L. Šmejkal, V. N. Strocov, P. Constantinou, A. B. Hellenes, R. Jaeschke Ubiergo, W. H. Campos, V. K. Bharadwaj, A. Chakraborty, *et al.*, Direct observation of altermagnetic band splitting in crsb thin films, *Nat. Commun.* **15**, 2116 (2024).
- [56] J. Ding, Z. Jiang, X. Chen, Z. Tao, Z. Liu, T. Li, J. Liu, J. Sun, J. Cheng, J. Liu, *et al.*, Large band splitting in g-wave altermagnet crsb, *Phys. Rev. Lett.* **133**, 206401 (2024).
- [57] G. Yang, Z. Li, S. Yang, J. Li, H. Zheng, W. Zhu, Z. Pan, Y. Xu, S. Cao, W. Zhao, *et al.*, Three-dimensional mapping of the altermagnetic spin splitting in crsb, *Nat. Commun.* **16**, 1442 (2025).
- [58] Z. Zhou, X. Cheng, M. Hu, R. Chu, H. Bai, L. Han, J. Liu, F. Pan, and C. Song, Manipulation of the altermagnetic order in crsb via crystal symmetry, *Nature* **638**, 645 (2025).
- [59] B. Jiang, M. Hu, J. Bai, Z. Song, C. Mu, G. Qu, W. Li, W. Zhu, H. Pi, Z. Wei, Y.-J. Sun, Y. Huang, X. Zheng, Y. Peng, L. He, S. Li, J. Luo, Z. Li, G. Chen, H. Li, H. Weng, and T. Qian, A metallic room-temperature d-wave altermagnet, *Nat. Phys.* **21**, 754 (2025).
- [60] F. Zhang, X. Cheng, Z. Yin, C. Liu, L. Deng, Y. Qiao, Z. Shi, S. Zhang, J. Lin, Z. Liu, M. Ye, Y. Huang, X. Meng, C. Zhang, T. Okuda, K. Shimada, S. Cui, Y. Zhao, G.-H. Cao, S. Qiao, J. Liu, and C. Chen, Crystal-symmetry-paired spin–valley locking in a layered room-temperature metallic altermagnet candidate, *Nat. Phys.* **21**, 760 (2025).
- [61] R. D. Gonzalez Betancourt, J. Zubáč, R. Gonzalez-Hernandez, K. Geishendorf, Z. Šobáň, G. Springholz, K. Olejník, L. Šmejkal, J. Sinova, T. Jungwirth, S. T. B. Goennenwein, A. Thomas, H. Reichlová, J. Železný, and D. Kriegner, Spontaneous anomalous hall effect arising from an unconventional compensated magnetic phase in a semiconductor, *Phys. Rev. Lett.* **130**, 036702 (2023).
- [62] S. Lee, S. Lee, S. Jung, J. Jung, D. Kim, Y. Lee, B. Seok, J. Kim, B. G. Park, L. Šmejkal, *et al.*, Broken kramers degeneracy in altermagnetic mnte, *Phys. Rev. Lett.* **132**, 036702 (2024).
- [63] J. Krempaský, L. Šmejkal, S. D’souza, M. Hajlaoui, G. Springholz, K. Uhlřřová, F. Alarab, P. Constantinou, V. Strocov, D. Usanov, *et al.*, Altermagnetic lifting of kramers spin degeneracy, *Nature* **626**, 517 (2024).
- [64] T. Osumi, S. Souma, T. Aoyama, K. Yamauchi, A. Honma, K. Nakayama, T. Takahashi, K. Ohgushi, and T. Sato, Observation of a giant band splitting in altermagnetic mnte, *Phys. Rev. B* **109**, 115102 (2024).
- [65] I. I. Mazin, K. Koepernik, M. D. Johannes, R. González-Hernández, and L. Šmejkal, Prediction of unconventional magnetism in doped fesb2, *Proc. Natl. Acad. Sci. U.S.A.* **118**, e2108924118 (2021).
- [66] L. Attias, A. Levchenko, and M. Khodas, Intrinsic anomalous hall effect in altermagnets, *Phys. Rev. B* **110**, 094425 (2024).
- [67] C. Phillips, G. Pokharel, K. Shtefienko, S. R. Bhandari, D. E. Graf, D. Rai, and K. Shrestha, Electronic structure of the altermagnet candidate fesb2: High-field torque magnetometry and density functional theory studies, *Phys. Rev. B* **111**, 075141 (2025).
- [68] L. Han, X. Fu, R. Peng, X. Cheng, J. Dai, L. Liu, Y. Li, Y. Zhang, W. Zhu, H. Bai, *et al.*, Electrical 180 switching of néel vector in spin-splitting antiferromagnet, *Sci. Adv.* **10**, eadn0479 (2024).
- [69] H. Reichlova, R. Lopes Seeger, R. González-Hernández, I. Kounta, R. Schlitz, D. Kriegner, P. Ritzinger, M. Lamme, M. Leiviskä, A. Birk Hellenes, *et al.*, Observation of a spontaneous anomalous hall response in the mn5si3 d-wave altermagnet candidate, *Nat. Commun.* **15**, 4961 (2024).
- [70] A. Badura, W. H. Campos, V. K. Bharadwaj, I. Kounta, L. Michez, M. Petit, J. Rial, M. Leiviskä, V. Baltz, F. Krizek, *et al.*, Observation of the anomalous nernst effect in altermagnetic candidate mn5si3, *Nat. Commun.* **16**, 7111 (2025).
- [71] S. Onoda, N. Sugimoto, and N. Nagaosa, Quantum transport theory of anomalous electric, thermoelectric, and thermal hall effects in ferromagnets, *Phys. Rev. B* **77**, 165103 (2008).
- [72] N. Nagaosa, J. Sinova, S. Onoda, A. H. MacDonald, and N. P. Ong, Anomalous hall effect, *Rev. Mod. Phys.* **82**, 1539 (2010).
- [73] S. Sun, Z. Song, H. Weng, and X. Dai, Topological metals induced by the zeeman effect, *Phys. Rev. B* **101**, 125118 (2020).
- [74] T. P. Cysne, S. Bhowal, G. Vignale, and T. G. Rapoport, Orbital hall effect in bilayer transition metal dichalcogenides: From the intra-atomic approximation to the bloch states orbital magnetic moment approach, *Phys. Rev. B* **105**, 195421 (2022).
- [75] B. Göbel and I. Mertig, Orbital hall effect accompanying quantum hall effect: Landau levels cause orbital polarized edge currents, *Phys. Rev. Lett.* **133**, 146301 (2024).